Spin-wave localization and guiding by magnon band structure engineering in yttrium iron garnet

Rouven Dreyer, Niklas Liebing, Eric R. J. Edwards,* Andreas Müller, and Georg Woltersdorf†
Institute of Physics, Martin Luther University Halle-Wittenberg, 06120 Halle, Germany

(Received 2 March 2021; accepted 1 June 2021; published 21 June 2021)

In spintronics, the propagation of spin-wave excitations in magnetically ordered materials can also be used to transport and process information. One of the most popular materials in this regard is the ferrimagnetic insulator yttrium iron garnet due its exceptionally small spin-wave damping parameter. While the small relaxation rate allows for large propagation length of magnetic excitations, it also leads to nonlocality of the magnetic properties. By imaging spin waves, their band structure is mapped with high-frequency resolution using a magneto-optic super-Nyquist sampling technique. In doing so, wave-vector selection is shown to suppress dispersion effects to a large extent, allowing for local measurements of spin relaxation. Moreover, we demonstrate even higher control of magnon propagation by employing the wave-vector selectivity near an avoided crossing of different spin-wave modes where the group velocity approaches zero. Here the local engineering of the dispersion allows us to construct magnonic waveguides, and at the same time it reveals the local relaxation properties.

DOI: 10.1103/PhysRevMaterials.5.064411

In recent years, spin-wave propagation and its control have been an intensely studied topic [1,2]. In parallel, it has been demonstrated that spin waves may be used to transport heat [3] and angular momentum [4]. In many of these experiments, yttrium iron garnet (YIG) has proven to be a valuable material. The insulating properties of YIG were used in YIG/metal hybrid structures to demonstrate a flurry of magnetoresistive and magnetothermal phenomena, which are explained by the excitation or annihilation of spin waves in YIG [5–9]. At the same time, the exceptionally small Gilbert damping constant of only $\alpha = 5 \times 10^{-5}$ of YIG enables spin transport on the millimeter length scale [3,10]. In most cases, the presence of magnon excitations in YIG can be probed on the nanoscale by the inverse spin Hall effect [6,11,12]. However, this approach is not sensitive to the properties of the spin wave that is converted into a signal, i.e., its wavelength and propagation direction. Magnetization dynamics at the micro- and nanoscale can be studied inductively [13–17] or by optical methods. Four distinct optical approaches are typically used: (i) microfocus Brillouin light scattering (μBLS) [18–23], (ii) time-resolved scanning transmission x-ray microscopy (TR-STXM) [24–26], (iii) time-resolved magneto-optic Kerr microscopy (TR-MOKE) [27–33], and (iv) diamond nitrogen-vacancy (NV) center resonance imaging [34–37]. The long spin-wave relaxation times in YIG complicate the analysis since extrinsic effects such as sample inhomogeneity, magnon-magnon scattering [38], or instrumental effects related to the excitation of multiple spin-wave modes or limited frequency resolution usually dominate the measured linewidth [39]. On the other hand, the large spin-wave propagation length allows to investigate coupling phenomena such as avoided crossings in the spin-wave dispersion in single YIG films [40,41] or YIG-based heterostructures [42–44]. In such systems, the strong-coupling regime between different magnon modes is accessible [45], paving the way for a novel playground for coherent information processing based on magnons [46]. Due to the large propagation lengths in YIG, it is difficult to confine spin waves. Usually, confinement is only achieved by physically patterning (e.g., dry-etching) the YIG material. Unfortunately, this approach introduces defects and modifies the magnetostatic properties. Therefore, for a number of experiments it would be highly desirable to have a method at hand allowing us to control the spin-wave properties locally without the need for patterning of the YIG structures.

In this article, we study the properties of spin waves in thin YIG layers by phase-resolved magneto-optic imaging of coherently excited spin waves. To reach the required frequency resolution and sensitivity for experiments with YIG, a modified version of the TR-MOKE method is introduced. In addition to the direct measurement of the spin-wave dispersion and avoided crossings of different spin-wave modes, we demonstrate that a truly local measurement of spin-wave relaxation properties becomes possible. In addition, by extracting group velocities and relaxation times of the excited spin waves near an avoided spin-wave mode crossing, we obtain an independent estimate for the local Gilbert damping parameter. Finally, we engineer the spin-wave dispersion locally to construct a soft magnonic waveguide, which allows us to study spin-wave propagation inside the spin-wave band gap opened by an avoided crossing of different spin-wave modes.

In our experiments, we perform TR-MOKE experiments on a 200-nm-thick YIG layer. The magnetization is excited coherently using the rf-field generated by a coplanar waveguide (CPW) patterned on top of the YIG layer [as shown in Fig. 1(a)]. The wave-vector spectrum of the excited spin waves is determined by the static in-plane magnetic field as

*Present address: IBM T. J. Watson Research Center, Yorktown Heights, New York 10598, USA.
†georg.woltersdorf@physik.uni-halle.de

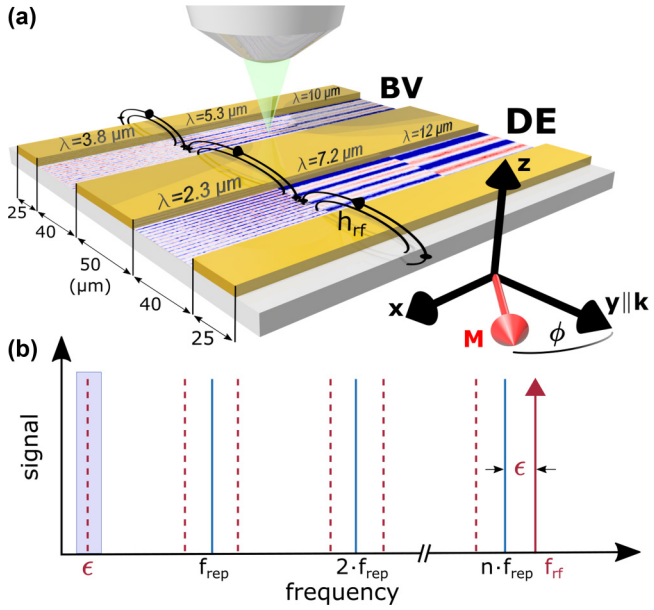

FIG. 1. (a) Geometry of the experiments. Spatial resolved images of spin waves in DE and BV configurations with their corresponding wavelength are shown in the gap. (b) The frequency comb generated by a femtosecond laser is given by multiples of the laser repetition rate f_{rep}. The excitation frequency f_{rf} aliases back to the Nyquist frequencies (red dotted lines). The lowest aliasing frequency corresponds to the difference frequency ε between f_{rf} and the nearest comb line.

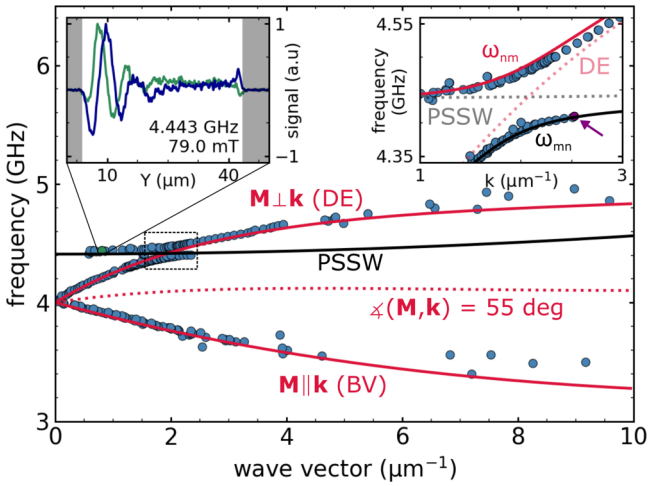

FIG. 2. Extracted spin-wave dispersion for a fixed external field of 79 mT. The dispersion curves were computed with the recipe by Kalinikos and Slavin [40,58] as discussed in the supplemental material. The red solid lines indicate the DE and BV dispersion. The dotted red line shows an angular orientation of nearly flat dispersion. The black solid line depicts the dispersion branch for the first PSSW. The top left inset shows the spin-wave profile in the vicinity of the avoided mode crossing recorded in the gap of the CPW. The top right inset shows a magnified view of the avoided mode crossing with the calculated mode repulsion [40,58].

well as the frequency and spatial distribution of the excitation field. We distinguish between the Damon-Eshbach (DE) and backward volume (BV) configurations as limiting cases of the in-plane dispersion [40], cf. supplemental Fig. S1 [47]. As a light source, a femtosecond laser operating at 510 nm with a repetition rate of $f_{rep} = 80$ MHz is used to sample the magnetization dynamics via the polar magneto-optical Kerr effect (MOKE), as shown in supplemental Fig. S2 [47]. Due to the small spin relaxation, studying spin waves in YIG requires a method with a frequency resolution on the order of 1 MHz. To meet this requirement, we introduce a measurement scheme that we term super-Nyquist sampling MOKE (SNS-MOKE). The MOKE effect allows for mixing of the excitation frequency f_{rf} and the nth harmonic of the laser pulse-repetition frequency yielding an intermediate frequency $f_{rf} = nf_{rep} + \varepsilon$. Demodulating the Kerr signal at frequency ε directly yields real and imaginary components of the magnetic rf-susceptibility, and in doing so it provides phase-resolved measurements of the spin precession (see the supplemental material [47] for details). Clearly, the advantage of the SNS-MOKE technique is that it allows for tuning of the rf-frequency in arbitrary steps. This is an enormous improvement over conventional pump-probe microscopy, where the frequency resolution is given by the laser repetition rate (i.e., 80 MHz in our case). Previously, we have used the SNS-MOKE technique only at fixed frequencies to image spin-wave modes [31,48,49].

Typical data of the spatially resolved, complex susceptibility are shown in Fig. 1(a) and recorded in DE and BV configurations, respectively. Here the external magnetic field is fixed at 142 mT and the rf-frequency is varied from image to image. The excited wave vector is determined by the maximum of the product of the **k**-dependent rf-magnetic field and rf-magnetic susceptibility $h(\mathbf{k}) \times \chi(\omega, \mathbf{k})$ [39], and it can be determined by counting the number of maxima n observed over distance L and calculating the wave number as $|\mathbf{k}| = 2\pi n/L$. In the following, we use the spin-wave wavelengths $\lambda = |\mathbf{k}|/2\pi$ determined from spatially resolved images [Fig. 1(a)] or line scans to map out the dispersion of BV and DE modes by extracting the wave vectors as a function of frequency for a fixed magnetic field, as shown in Fig. 2. Using the SNS-MOKE method, we are able to map out the spin-wave dispersion with a pronounced avoided crossing [24,50–53] using a step size of only 2 MHz, as shown in the inset of Fig. 2.

The avoided crossing of the first-order perpendicular standing spin-wave mode (PSSW) and the DE mode has a much larger frequency splitting than the linewidth of individual spin-wave modes involved, indicating strong coupling. Following the formalism introduced by Kalinikos and Slavin [40,54], we determine the mode repulsion of DE and first-order PSSW mode and the corresponding size of the frequency splitting (see supplemental Fig. S3 [47]). In particular, we obtain a coupling constant $g = f_{splitting}/(\Delta f_1 + \Delta f_2)$ of 220 at 4 GHz from the experiment. Note that values larger than $g = 1$ are referred to as strong coupling [55], and they allow for coherent exchange of information between the two modes. The solid lines in Fig. 2 show the calculated dispersion for DE, BV (red), and PSSW (black) modes. In Fig. 2, the left inset shows the observed spatial profile of one of the hybridized modes in the vicinity of the avoided crossing. Here the propagation of the spin wave is strongly suppressed in

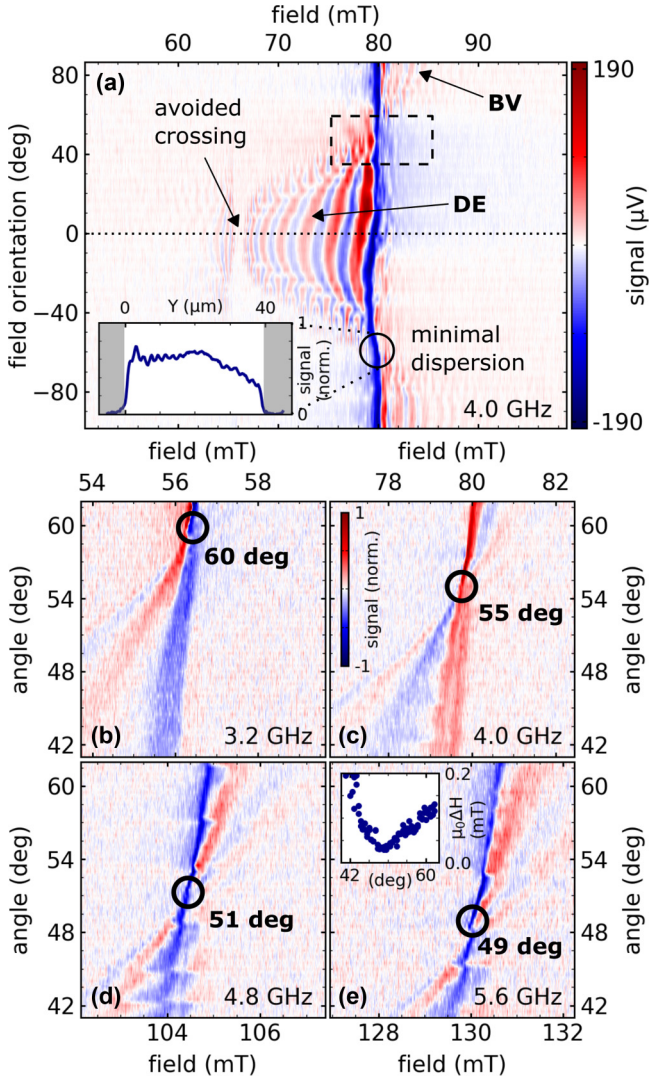

FIG. 3. (a) Angular dependence of the local field swept measurements of the rf-susceptibility measured with an excitation frequency of 4.0 GHz. A clear minimum of the dispersion around a magnetic field direction of 55 degrees is visible. The inset shows the nearly uniform spatial distribution of the magnetic excitation across the gap recorded at the dispersion minimum. (b)–(e) Detailed measurement of the spin-wave dispersion minimum for frequencies between 3 and 6 GHz. The inset in panel (e) depicts the extracted linewidth of the 5.6 GHz measurement as a function of in-plane field orientation clearly showing a minimum at nearly flat dispersion.

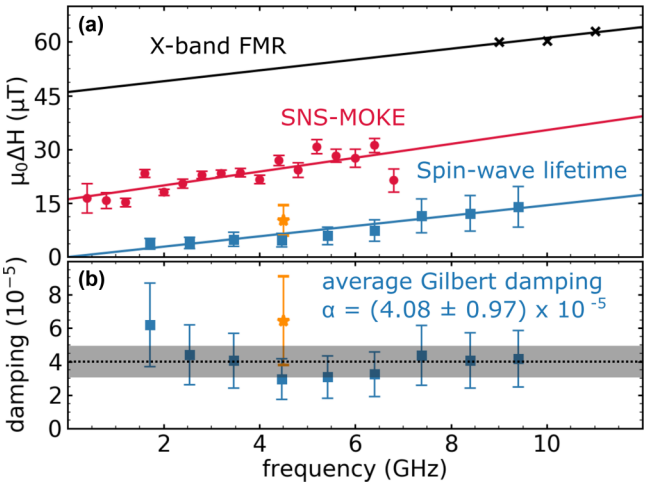

FIG. 4. (a) Frequency dependence of the linewidth for FMR measurements (black cross) and at the dispersion minimum (red dots). The blue data points show the calculated linewidth in the vicinity of the avoided crossing. Solid lines are fits to extract the Gilbert damping. (b) Gilbert damping for localized spin-wave modes for different frequency. The dotted black line indicates the average damping parameter, while the gray area is the standard deviation. The orange star marks the data point taken within the magnonic waveguide presented in Fig. 5(d).

comparison to the maps shown in Fig. 1(a). We attribute this effect to the nearly flat dispersion and therefore small group velocity close to the anticrossing. Specifically, the spin-wave group velocity is reduced from 200 m/s to values of about 10 m/s near the mode repulsion (indicated by the purple arrow in the right inset of Fig. 2).

The Gilbert damping parameter is usually determined from the linewidth by sweeping the magnetic field at a fixed frequency across the ferromagnetic resonance (FMR). In Fig. 3 we record the SNS-MOKE signal in two-dimensional plots as a function of in-plane magnetic field magnitude and in-plane orientation. As one can see, e.g., by following the signal along the dotted line, locally measured field sweeps are not suitable to determine the Gilbert damping (cf. supplemental Fig. S1 [47]). To evaluate these spectra, it would be necessary to take the wave-vector distribution of the excitation field, the dispersion, and the spin-wave propagation effects properly into account [56]. One might overcome this problem by identifying the magnetization direction where the dispersion is nearly flat and the spin waves cannot propagate. A nearly flat dispersion is expected for an intermediate angle of the field orientation between BV and DE configurations where the different dipolar contributions compensate each other (red dotted line in Fig. 2). The actual angle where the dispersion becomes nearly flat is indicated by black circles in Fig. 3 and depends on the rf-frequency (Fig. S4 [47]). A flat dispersion results in the simultaneous excitation of spin waves of all excited wave vectors, causing destructive interference of all spin-wave modes except for the uniform mode ($k = 0$). This behavior is indeed observed in the inset of Fig. 3(a), where mostly a uniform precession of the magnetization occurs. At 4 GHz, a flat dispersion is expected for an angle between $\mathbf{k}$ and $\mathbf{M}$ of 55 degrees as indicated in Fig. 2. In addition, because the dispersion is flat, the excited spin waves have a nearly vanishing group velocity $v_g = \partial\omega/\partial\mathbf{k}$ and cannot propagate. As demonstrated in the inset of Fig. 3(e), a pronounced minimum of the resonance linewidth is indeed observed for these conditions. By measuring the susceptibility at the angles of minimal dispersion, we extract Lorentzian resonance line shapes from the local SNS-MOKE spectra that can be easily interpreted in terms of their linewidth. Figure 4(a) shows the frequency-dependent linewidth determined from a series of such spectra obtained in the point of minimal dispersion. The Gilbert damping determined from the red data points in Fig. 4(a) corresponds to a value of $\alpha = (5.41 \pm 1.07) \times 10^{-5}$ with a very small zero-frequency linewidth offset ΔH_0 of only

16 μT and hence three times smaller compared to conventional FMR measurements we performed on the same sample. The remaining zero-frequency linewidth offset is most likely caused by two-magnon scattering processes, which are facilitated by a flat dispersion extending to large **k**-vectors.

An even better localization of the probed properties may be achieved by controlling the magnon band structure such that degenerate magnon modes can be avoided completely. In the following, we will look in detail at the presented avoided crossing, and in doing so study spin waves with tunable propagation length with the aim to localize them. The associated change in curvature of the dispersion offers a handle to control the magnon propagation length since it is given by the product of spin-wave lifetime and group velocity [39]: $\lambda_{\mathrm{prop}} = \tau v_{\mathrm{g}}$, where the lifetime [57] is related to the Gilbert damping parameter by

$$\tau = \frac{2}{\alpha} \frac{1}{\gamma \mu_0 (M_0 + H)}. \tag{1}$$

Obviously, in the case of a flat dispersion, the probed signal has a truly local character and provides access to intrinsic local properties such as internal fields and the Gilbert damping parameter. In the region of mode repulsion, the excited spin-wave modes are localized close to the edges of the conductors of the CPW (left inset in Fig. 2). Using different frequencies and a nearly flat dispersion found in the vicinity of the avoided mode crossing (shown in supplemental Fig. S3 [47]) we extract the propagation length λ_{prop} and the group velocity v_g for these modes and calculate an average Gilbert damping parameter of $\alpha = (4.08 \pm 0.97) \times 10^{-5}$ for frequencies between 1 and 8 GHz using the equation above. The narrow linewidths for different frequencies [Fig. 4(a)] and the corresponding Gilbert damping parameters [Fig. 4(b)] calculated from the obtained data are a consequence of the local character of the damping measurement under nearly flat dispersion conditions.

In the following, we will demonstrate that the magnon band gap at small wave vectors created by the avoided crossing allows us to realize magnon guiding along a track defined by tiny local fields. One can set the external field and the excitation frequency such that no spin waves can be excited and propagate [gray shaded area in, e.g., Fig. 5(a)]. To locally guide spin waves along a predefined track, it is required to locally shift this band gap. For this we define magnetic structures on top of the YIG layer in order to provide a local bias field in their gap, as shown in Figs. 5(c) and 5(d). The local in-plane stray field amounts to ~0.5 mT for 10-nm-thick Permalloy structures with a 5 μm gap, and it induces a shift of the magnon dispersion of about 100 MHz [Fig. 5(b)]. Now one can select a frequency where the spin-wave propagation within the magnonic waveguide is still allowed while it is forbidden due to the magnon band gap in the surrounding magnetic material. This situation is demonstrated in Fig. 5(d) for a frequency of 4.45 GHz and an applied external field of 79 mT. The spin-wave mode within the magnonic waveguide can propagate over several 10 μm while the propagation on the left and right side of the waveguide is evanescent. By determining the decay length of this specific spin-wave mode and the corresponding group velocity from the dispersion, we find a Gilbert damping parameter of $\alpha = (6.4 \pm 1.3) \times 10^{-5}$

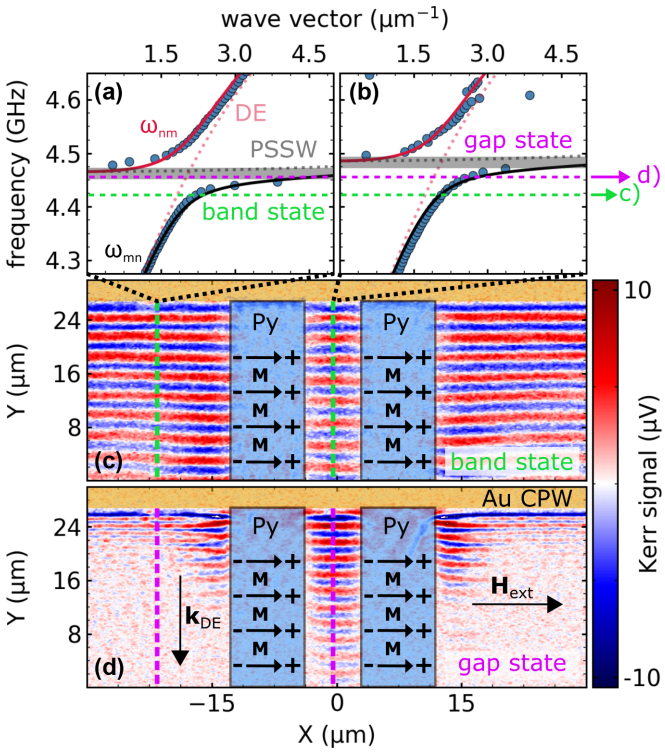

FIG. 5. Parts (a) and (b) show the magnonic band gap for an external field of 79 mT at positions next to and within the magnonic waveguide, respectively. In (b) the dispersion is slightly shifted toward larger frequencies. Here we find a regime where in contrast to the band state in (c), the propagation of DE spin-wave modes is only possible within the waveguide (gap state) as observed in (d).

(and we calculate a linewidth of 10.3 ± 2.1 μT) (both indicated by orange stars in Fig. 4).

In summary, we demonstrate that by selecting the orientation of the wave vector, it is possible to avoid spin-wave dispersion to a large extent. Even more interestingly, strong modification of the dispersion in the vicinity of the avoided crossing allows us to select arbitrarily low values of the spin-wave velocity and hence to address the Gilbert damping locally. Using the exceptional frequency resolution of the SNS-MOKE technique introduced here, we show that the spin-wave interaction in the vicinity of the mode crossing represents a case of strong coupling, allowing us to study cooperative phenomena such as Rabi oscillations for spin-wave excitations as well in the future. Finally, we demonstrated that a forbidden magnon band can be created by the avoided crossing. By local modification of the dispersion using the stray field of magnetic microstructures, we have designed a "soft" magnonic waveguide. This waveguide supports spin waves in the vicinity of the avoided crossing, while the propagation in the surrounding material is forbidden. Due to the low Gilbert damping, tiny local bias fields are sufficient to control the propagation properties. In the future, such magnetic fields may be generated by currents flowing in microfabricated wire structures placed on top of the YIG layer, allowing for a dynamic control of magnon propagation.

Financial support from the German research foundation (DFG) through collaborative research center (CRC)/TRR

227 and Priority Program SPP 1538 (Spin Caloric Transport) as well as from the European Research Council (ERC) via starting Grant No. 280048 (ECOMAGICS) is gratefully acknowledged.

[1] V. V. Kruglyak, S. O. Demokritov, and D. Grundler, Magnonics, J. Phys. D **43**, 264001 (2010).

[2] A. V. Chumak, V. I. Vasyuchka, A. A. Serga, and B. Hillebrands, Magnon spintronics, Nat. Phys. **11**, 453 (2015).

[3] T. An, V. I. Vasyuchka, K. Uchida, A. V. Chumak, K. Yamaguchi, K. Harii, J. Ohe, M. B. Jungfleisch, Y. Kajiwara, H. Adachi, B. Hillebrands, S. Maekawa, and E. Saitoh, Unidirectional spin-wave heat conveyer, Nat. Mater. **12**, 549 (2013).

[4] Y. Kajiwara, K. Harii, S. Takahashi, J. Ohe, K. Uchida, M. Mizuguchi, H. Umezawa, H. Kawai, K. Ando, K. Takanashi, S. Maekawa, and E. Saitoh, Transmission of electrical signals by spin-wave interconversion in a magnetic insulator, Nature **464**, 262 (2010).

[5] K. Uchida, H. Adachi, T. An, T. Ota, M. Toda, B. Hillebrands, S. Maekawa, and E. Saitoh, Long-range spin Seebeck effect and acoustic spin pumping, Nat. Mater. **10**, 737 (2011).

[6] H. Nakayama, M. Althammer, Y. T. Chen, K. Uchida, Y. Kajiwara, D. Kikuchi, T. Ohtani, S. Geprägs, M. Opel, S. Takahashi, R. Gross, G. E. W. Bauer, S. T. B. Goennenwein, and E. Saitoh, Spin Hall Magnetoresistance Induced by a Nonequilibrium Proximity Effect, Phys. Rev. Lett. **110**, 206601 (2013).

[7] L. J. Cornelissen, J. Liu, R. A. Duine, J. B. Youssef, and B. J. van Wees, Long-distance transport of magnon spin information in a magnetic insulator at room temperature, Nat. Phys. **11**, 1022 (2015).

[8] J. Li, Y. Xu, M. Aldosary, C. Tang, Z. Lin, S. Zhang, R. Lake, and J. Shi, Observation of magnon-mediated current drag in Pt/yttrium iron garnet/Pt(Ta) trilayers, Nat. Commun. **7**, 10858 (2016).

[9] M. Evelt, C. Safranski, M. Aldosary, V. E. Demidov, I. Barsukov, A. P. Nosov, A. B. Rinkevich, K. Sobotkiewich, X. Li, J. Shi, I. N. Krivorotov, and S. O. Demokritov, Spin Hall-induced auto-oscillations in ultrathin YIG grown on Pt, Sci. Rep. **8**, 1269 (2018).

[10] C. Hauser, T. Richter, N. Homonnay, C. Eisenschmidt, M. Qaid, H. Deniz, D. Hesse, M. Sawicki, S. G. Ebbinghaus, and G. Schmidt, Yttrium iron garnet thin films with very low damping obtained by recrystallization of amorphous material, Sci. Rep. **6**, 20827 (2016).

[11] M. Weiler, M. Althammer, F. D. Czeschka, H. Huebl, M. S. Wagner, M. Opel, I.-M. Imort, G. Reiss, A. Thomas, R. Gross, and S. T. B. Goennenwein, Local charge and spin currents in magnetothermal landscapes, Phys. Rev. Lett. **108**, 106602 (2012).

[12] M. Collet, X. de Milly, O. d'Allivy Kelly, V. V. Naletov, R. Bernard, P. Bortolotti, J. Ben Youssef, V. E. Demidov, S. O. Demokritov, J. L. Prieto, M. Munoz, V. Cros, A. Anane, G. de Loubens, and O. Klein, Generation of coherent spin-wave modes in yttrium iron garnet microdiscs by spin-orbit torque, Nat. Commun. **7**, 10377 (2016).

[13] V. Vlaminck and M. Bailleul, Current-induced spin-wave doppler shift, Science **322**, 410 (2008).

[14] H. Yu, G. Duerr, R. Huber, M. Bahr, T. Schwarze, F. Brandl, and D. Grundler, Omnidirectional spin-wave nanograting coupler, Nat. Commun. **4**, 2702 (2013).

[15] H. Qin, S. J. Hämäläinen, K. Arjas, J. Witteveen, and S. van Dijken, Propagating spin waves in nanometer-thick yttrium iron garnet films: Dependence on wave vector, magnetic field strength, and angle, Phys. Rev. B **98**, 224422 (2018).

[16] P. Che, K. Baumgaertl, A. Kukol'ova, C. Dubs, and D. Grundler, Efficient wavelength conversion of exchange magnons below 100 nm by magnetic coplanar waveguides, Nat. Commun. **11**, 1445 (2020).

[17] H. J. Chia, F. Guo, L. M. Belova, and R. D. McMichael, Nanoscale Spin Wave Localization Using Ferromagnetic Resonance Force Microscopy, Phys. Rev. Lett. **108**, 087206 (2012).

[18] V. E. Demidov, J. Jersch, K. Rott, P. Krzysteczko, G. Reiss, and S. O. Demokritov, Nonlinear Propagation of Spin Waves in Microscopic Magnetic Stripes, Phys. Rev. Lett. **102**, 177207 (2009).

[19] V. E. Demidov, S. Urazhdin, H. Ulrichs, V. Tiberkevich, A. Slavin, D. Baither, G. Schmitz, and S. O. Demokritov, Magnetic nano-oscillator driven by pure spin current, Nat. Mater. **11**, 1028 (2012).

[20] K. Vogt, F. Y. Fradin, J. E. Pearson, T. Sebastian, S. D. Bader, B. Hillebrands, A. Hoffmann, and H. Schultheiss, Realization of a spin-wave multiplexer, Nat. Commun. **5**, 3727 (2014).

[21] K. Vogt, H. Schultheiss, S. Jain, J. E. Pearson, A. Hoffmann, S. D. Bader, and B. Hillebrands, Spin waves turning a corner, Appl. Phys. Lett. **101**, 042410 (2012).

[22] M. Collet, O. Gladii, M. Evelt, V. Bessonov, L. Soumah, P. Bortolotti, S. O. Demokritov, Y. Henry, V. Cros, M. Bailleul, V. E. Demidov, and A. Anane, Spin-wave propagation in ultra-thin YIG based waveguides, Appl. Phys. Lett. **110**, 092408 (2017).

[23] T. Hache, M. Vaňatka, L. Flajšman, T. Weinhold, T. Hula, O. Ciubotariu, M. Albrecht, B. Arkook, I. Barsukov, L. Fallarino, O. Hellwig, J. Fassbender, M. Urbánek, and H. Schultheiss, Freestanding Positionable Microwave-Antenna Device for Magneto-Optical Spectroscopy Experiments, Phys. Rev. Appl. **13**, 054009 (2020).

[24] J. Förster, S. Wintz, J. Bailey, S. Finizio, E. Josten, C. Dubs, D. A. Bozhko, H. Stoll, G. Dieterle, N. Träger, J. Raabe, A. N. Slavin, M. Weigand, J. Gräfe, and G. Schütz, Nanoscale X-ray imaging of spin dynamics in yttrium iron garnet, J. Appl. Phys. **126**, 173909 (2019).

[25] K. Baumgaertl, J. Grafe, P. Che, A. Mucchietto, J. Forster, N. Trager, M. Bechtel, M. Weigand, G. Schutz, and D. Grundler, Nanoimaging of ultrashort magnon emission by ferromagnetic grating couplers at GHz frequencies, Nano Lett. **20**, 7281 (2020).

[26] V. Sluka, T. Schneider, R. A. Gallardo, A. Kakay, M. Weigand, T. Warnatz, R. Mattheis, A. Roldan-Molina, P. Landeros, V. Tiberkevich, A. Slavin, G. Schutz, A. Erbe, A. Deac, J. Lindner, J. Raabe, J. Fassbender, and S. Wintz, Emission and propagation of 1D and 2D spin waves with nanoscale wavelengths in anisotropic spin textures, Nat. Nanotechnol. **14**, 328 (2019).

[27] J.-Y. Chauleau, H. G. Bauer, H. S. Körner, J. Stigloher, M. Härtinger, G. Woltersdorf, and C. H. Back, Self-consistent determination of the key spin-transfer torque parameters from

spin-wave Doppler experiments, Phys. Rev. B **89**, 020403(R) (2014).

[28] J. P. Park and P. A. Crowell, Interactions of Spin Waves with a Magnetic Vortex, Phys. Rev. Lett. **95**, 167201 (2005).

[29] Z. Liu, F. Giesen, X. Zhu, R. D. Sydora, and M. R. Freeman, Spin Wave Dynamics and the Determination of Intrinsic Damping in Locally Excited Permalloy Thin Films, Phys. Rev. Lett. **98**, 087201 (2007).

[30] H. T. Nembach, J. M. Shaw, C. T. Boone, and T. J. Silva, Mode- and Size-Dependent Landau-Lifshitz Damping in Magnetic Nanostructures: Evidence for Nonlocal Damping, Phys. Rev. Lett. **110**, 117201 (2013).

[31] F. Heyroth, C. Hauser, P. Trempler, P. Geyer, F. Syrowatka, R. Dreyer, S. G. Ebbinghaus, G. Woltersdorf, and G. Schmidt, Monocrystalline Freestanding Three-Dimensional Yttrium-Iron-Garnet Magnon Nanoresonators, Phys. Rev. Appl. **12**, 054031 (2019).

[32] G. Woltersdorf, O. Mosendz, B. Heinrich, and C. H. Back, Magnetization Dynamics Due to Pure Spin Currents in Magnetic Double Layers, Phys. Rev. Lett. **99**, 246603 (2007).

[33] J. Stigloher, M. Decker, H. S. Körner, K. Tanabe, T. Moriyama, T. Taniguchi, H. Hata, M. Madami, G. Gubbiotti, K. Kobayashi, T. Ono, and C. H. Back, Snell's Law for Spin Waves, Phys. Rev. Lett. **117**, 037204 (2016).

[34] C. Du, T. van der Sar, T. X. Zhou, P. Upadhyaya, F. Casola, H. Zhang, M. C. Onbasli, C. A. Ross, R. L. Walsworth, Y. Tserkovnyak, and A. Yacoby, Control and local measurement of the spin chemical potential in a magnetic insulator, Science **357**, 195 (2017).

[35] I. Bertelli, J. J. Carmiggelt, T. Yu, B. G. Simon, C. C. Pothoven, G. E. W. Bauer, Y. M. Blanter, J. Aarts, and T. van der Sar, Magnetic resonance imaging of spin-wave transport and interference in a magnetic insulator, Sci. Adv. **6**, eabd3556 (2020).

[36] E. Lee-Wong, R. Xue, F. Ye, A. Kreisel, T. van der Sar, A. Yacoby, and C. R. Du, Nanoscale detection of magnon excitations with variable wavevectors through a quantum spin sensor, Nano Lett. **20**, 3284 (2020).

[37] B. A. McCullian, A. M. Thabt, B. A. Gray, A. L. Melendez, M. S. Wolf, V. L. Safonov, D. V. Pelekhov, V. P. Bhallamudi, M. R. Page, and P. C. Hammel, Broadband multi-magnon relaxometry using a quantum spin sensor for high frequency ferromagnetic dynamics sensing, Nat. Commun. **11**, 5229 (2020).

[38] R. D. McMichael, D. J. Twisselmann, and A. Kunz, Localized Ferromagnetic Resonance in Inhomogeneous Thin Films, Phys. Rev. Lett. **90**, 227601 (2003).

[39] H. G. Bauer, J. Y. Chauleau, G. Woltersdorf, and C. H. Back, Coupling of spinwave modes in wire structures, Appl. Phys. Lett. **104**, 102404 (2014).

[40] B. A. Kalinikos and A. N. Slavin, Theory of dipole-exchange spin wave spectrum for ferromagnetic films with mixed exchange boundary conditions, J. Phys. C **19**, 7013 (1986).

[41] R. Henry, S. D. Brown, P. E. Wigen, and P. J. Besser, Magnetoexchange Branch Repulsion in Thin Single-Crystal Disks of Yttrium Iron Garnet, Phys. Rev. Lett. **28**, 1272 (1972).

[42] H. Qin, S. J. Hamalainen, and S. van Dijken, Exchange-torque-induced excitation of perpendicular standing spin waves in nanometer-thick YIG films, Sci. Rep. **8**, 5755 (2018).

[43] J. Chen, C. Liu, T. Liu, Y. Xiao, K. Xia, G. E. W. Bauer, M. Wu, and H. Yu, Strong Interlayer Magnon-Magnon Coupling in Magnetic Metal-Insulator Hybrid Nanostructures, Phys. Rev. Lett. **120**, 217202 (2018).

[44] S. Klingler, V. Amin, S. Geprags, K. Ganzhorn, H. Maier-Flaig, M. Althammer, H. Huebl, R. Gross, R. D. McMichael, M. D. Stiles, S. T. B. Goennenwein, and M. Weiler, Spin-Torque Excitation of Perpendicular Standing Spin Waves in Coupled YIG/Co Heterostructures, Phys. Rev. Lett. **120**, 127201 (2018).

[45] Y. Li, W. Cao, V. P. Amin, Z. Zhang, J. Gibbons, J. Sklenar, J. Pearson, P. M. Haney, M. D. Stiles, W. E. Bailey, V. Novosad, A. Hoffmann, and W. Zhang, Coherent Spin Pumping in a Strongly Coupled Magnon-Magnon Hybrid System, Phys. Rev. Lett. **124**, 117202 (2020).

[46] Y. Li, W. Zhang, V. Tyberkevych, W.-K. Kwok, A. Hoffmann, and V. Novosad, Hybrid magnonics: Physics, circuits, and applications for coherent information processing, J. Appl. Phys. **128**, 130902 (2020).

[47] See Supplemental Material at http://link.aps.org/supplemental/10.1103/PhysRevMaterials.5.064411 for additional details regarding the SNS-MOKE technique, frequency-dependent change of minimal dispersion, and the utilized model for calculating the avoided mode.

[48] P. Trempler, R. Dreyer, P. Geyer, C. Hauser, G. Woltersdorf, and G. Schmidt, Integration and characterization of micron-sized YIG structures with very low Gilbert damping on arbitrary substrates, Appl. Phys. Lett. **117**, 232401 (2020).

[49] H. Qin, R. B. Hollander, L. Flajsman, F. Hermann, R. Dreyer, G. Woltersdorf, and S. van Dijken, Nanoscale magnonic Fabry-Perot resonator for low-loss spin-wave manipulation, Nat. Commun. **12**, 2293 (2021).

[50] P. Kabos, W. D. Wilber, C. E. Patton, and P. Grünberg, Brillouin light scattering study of magnon branch crossover in thin iron films, Phys. Rev. B **29**, 6396 (1984).

[51] J. Jorzick, S. O. Demokritov, C. Mathieu, B. Hillebrands, B. Bartenlian, C. Chappert, F. Rousseaux, and A. N. Slavin, Brillouin light scattering from quantized spin waves in micron-size magnetic wires, Phys. Rev. B **60**, 15194 (1999).

[52] M. Wu, B. A. Kalinikos, and C. E. Patton, Generation of Dark and Bright Spin Wave Envelope Soliton Trains Through Self-Modulational Instability in Magnetic Films, Phys. Rev. Lett. **93**, 157207 (2004).

[53] S. Maendl, I. Stasinopoulos, and D. Grundler, Spin waves with large decay length and few 100 nm wavelengths in thin yttrium iron garnet grown at the wafer scale, Appl. Phys. Lett. **111**, 012403 (2017).

[54] B. A. Kalinikos, Spin-wave spectrum and linear excitation of spin-waves in ferromagnetic-films, Sov. Phys. J. **24**, 718 (1981).

[55] L. Novotny, Strong coupling, energy splitting, and level crossings: A classical perspective, Am. J. Phys. **78**, 1199 (2010).

[56] M. Farle, T. Silva, and G. Woltersdorf, *Spin Dynamics in the Time and Frequency Domain*, edited by H. Zabel and M. Farle, Springer Tracts in Modern Physics Vol. 246 (Springer, Berlin, 2013), pp. 37–83.

[57] G. Woltersdorf, M. Buess, B. Heinrich, and C. H. Back, Time Resolved Magnetization Dynamics of Ultrathin Fe(001) Films: Spin-pumping and Two-Magnon Scattering, Phys. Rev. Lett. **95**, 037401(2005).

[58] K. Perzlmaier, G. Woltersdorf, and C. H. Back, Observation of the propagation and interference of spin waves in ferromagnetic thin films, Phys. Rev. B **77**, 054425 (2008).